Computational Thermostabilization of an Enzyme

Aaron Korkegian, *et al.*

Science **308**, 857 (2005);
DOI: 10.1126/science.1107387

4. U. Neff *et al.*, *Nature* **411**, 290 (2001).
5. D. Fleitmann *et al.*, *Science* **300**, 1737 (2003).
6. R. Agnihotri, K. Dutta, R. Bhushan, B. L. K. Somayajulu, *Earth Planet. Sci. Lett.* **198**, 521 (2002).
7. Z. S. An, *Quat. Sci. Rev.* **19**, 171 (2000).
8. S. C. Porter, Z. S. An, *Nature* **375**, 305 (1995).
9. Y. J. Wang *et al.*, *Science* **294**, 2345 (2001).
10. C. A. Dykoski *et al.*, *Earth Planet. Sci. Lett.*, **233**, 71 (2005).
11. W. Dansgaard *et al.*, *Nature* **364**, 218 (1993).
12. P. M. Grootes, M. Stuiver, J. W. C. White, S. J. Johnsen, J. Jouzel, *Nature* **366**, 552 (1993).
13. North Greenland Ice Core Project Members, *Nature* **431**, 147 (2004).
14. D. Yuan *et al.*, *Science* **304**, 575 (2004).
15. M. Stuiver *et al.*, *Radiocarbon* **40**, 1041 (1998).
16. K. R. Johnson, B. L. Ingram, *Earth Planet. Sci. Lett.* **220**, 365 (2004).
17. G. Haug, K. A. Hughen, D. M. Sigman, L. C. Peterson, U. Röhl, *Science* **293**, 1304 (2001).
18. X. Wang *et al.*, *Nature* **432**, 740 (2004).
19. A. K. Gupta, D. M. Anderson, J. T. Overpeck, *Nature* **421**, 354 (2003).
20. J. U. L. Baldini, F. McDermott, I. J. Fairchild, *Science* **296**, 2203 (2002).
21. D. R. Rousseau, R. Precce, N. Limondin, *Geology* **26**, 651 (1998).
22. D. C. Barber *et al.*, *Nature* **400**, 344 (1999).
23. W. Wu, T. Liu, *Quat. Int.* **117**, 153 (2004).
24. Y. T. Hong *et al.*, *Earth Planet. Sci. Lett.* **211**, 371 (2003).
25. B. Peter, *Science* **292**, 667 (2001).
26. Eighty-two time-points were selected using a criterion of $\geq\pm 10$ ‰ fluctuation in atmospheric $\Delta^{14}C$ for tuning. The tuned DA time scale is within the ^{230}Th dating error. The tuned age-depth relation remains smooth and is essentially the same as the ^{230}Th dated age-depth relation (Fig. 1B).
27. M. Stuiver, T. Braziunas, *Holocene* **3**, 289 (1993).
28. D. T. Shindell, G. A. Schmidt, M. E. Mann, D. Rind, A. Waple, *Science* **294**, 2149 (2001).
29. Supported by National Science Foundation of China grants 40225007 and 40328005, FANEDD 200227, National Basic Research Program of China 2004CB720204, U.S. NSF Grants 0214041, 0116395, and 023239, and Gary Comer Science and Education Foundation Grant CC8. The Minnesota authors thank G. Comer and W. S. Broecker for their generous support.

Supporting Online Material
www.sciencemag.org/cgi/content/full/308/5723/854/DC1
Figs. S1 and S2
Tables S1 and S2
References

12 October 2004; accepted 3 March 2005
10.1126/science.1106296

Computational Thermostabilization of an Enzyme

Aaron Korkegian,[1,2] Margaret E. Black,[4] David Baker,[3] Barry L. Stoddard[1]*

Thermostabilizing an enzyme while maintaining its activity for industrial or biomedical applications can be difficult with traditional selection methods. We describe a rapid computational approach that identified three mutations within a model enzyme that produced a 10°C increase in apparent melting temperature T_m and a 30-fold increase in half-life at 50°C, with no reduction in catalytic efficiency. The effects of the mutations were synergistic, giving an increase in excess of the sum of their individual effects. The redesigned enzyme induced an increased, temperature-dependent bacterial growth rate under conditions that required its activity, thereby coupling molecular and metabolic engineering.

Enzymes are the most efficient catalysts of chemical reactions known, enhancing reaction rates by as much as 23 orders of magnitude (*1*, *2*). However, there has been little evolutionary pressure for them to become more thermostable than is required by their native environment. Many studies indicate that enzymes (like most proteins) exhibit closely balanced free energy profiles for folding and unfolding, thereby allowing functionally important dynamic motions and appropriate degradation in vivo (*3*). However, in a laboratory or industrial setting, this lack of thermostability can lead to undesirable loss of activity (*4*).

The physical principles of protein folding that result in a balance of stability and flexibility, while maintaining function, are not perfectly understood and have been difficult to exploit for the development of thermostabilized enzymes (*4*). For hyperthermophiles, selective pressures have generated proteins with denaturation temperatures upwards of 110°C (*5*). Their proteins exhibit topologies and stabilizing interactions similar to those from mesophilic and thermophilic organisms (*6*, *7*), leading to diverse hypotheses regarding their relative behaviors (*8*). However, a key mechanism for thermostabilization appears to be the optimization of interactions between amino acids within a protein's core (*5*), complementing computational design methods that optimize a sequence for a given fold (*9*–*13*).

The thermostabilization of an enzyme presents additional challenges for computational protein design methods, because the active-site substrate geometry and the molecular dynamic behavior during an enzymatic reaction often appear fine-tuned for maximum catalytic efficiency (*2*, *3*). Therefore, the design method must be capable of predicting thermostabilizing mutations within a given fold while minimizing any shift in the backbone that might structurally disrupt the active-site structure or quench its flexibility.

In the past several years, methods for computational protein structure prediction and design have improved substantially (*10*, *11*, *14*). Recently, computational design has been used successfully in thermostabilizing noncatalytic proteins (*15*–*18*), redesigning binding pockets (*19*–*23*), creating a protein fold (*24*), and designing catalytic activity into a bacterial receptor (*25*). We use the program RosettaDesign (*26*), which uses an energy function for evaluating the fitness of a particular sequence for a given fold and a Metropolis Monte Carlo search algorithm for sampling sequence space. The program requires a backbone structure as input and generates sequences that have the lowest energy for that fold.

We picked the homodimeric hydrolase enzyme yeast cytosine deaminase (yCD), which converts cytosine to uracil, as a target for computational thermostabilization. yCD was chosen because its high-resolution crystal structure is available (*27*), its catalytic mechanism is well characterized (*27*), it is thermolabile (*28*, *29*), and it has potential use in antitumor suicide gene applications (*27*, *29*–*31*). As do many commercially useful enzymes, yCD displays irreversible unfolding behavior at high temperatures (presumably because of aggregation) rather than the more simple, fully reversible behavior common among model systems for the study of protein folding. The problems inherent in engineering such catalysts have been recently reviewed (*4*). We used computational redesign to predict a series of point mutations in the enzyme core that might lead to thermostabilization of the enzyme without losing catalytic efficiency. We then prepared a series of designed enzyme variants and determined their folded thermostability, catalytic behavior, ability to complement metabolic cytosine deaminase activity, and three-dimensional crystal structures.

Our general computational strategy was largely unchanged from that described by Kuhlman and Baker (*26*, *32*). An energy function evaluated target sequences threaded onto a template backbone (*12*, *13*, *26*, *33*). Sequence space was searched with an iterative Metropolis Monte Carlo procedure, starting with a random sequence, replacing a single amino acid rotamer with a rotamer from the Dunbrack backbone-dependent rotamer library (*34*), and reevaluating the energy. Sequences with lower energy were automatically adopted, whereas

[1]Division of Basic Sciences, Fred Hutchinson Cancer Research Center (FHCRC), 1100 Fairview Avenue North, Seattle, WA 98109, USA. [2]Graduate Program in Molecular and Cellular Biology, [3]Department of Biochemistry and Howard Hughes Medical Institute, University of Washington, Seattle, WA 98195, USA. [4]Department of Pharmaceutical Sciences, College of Pharmacy, Washington State University, Pullman, WA 99164–6534, USA.

*To whom correspondence should be addressed. E-mail: bstoddar@fhcrc.org

sequences with higher energy were accepted with a probability based on the Metropolis criterion in order to prevent trapping in a local energy minimum.

All residues directly involved in catalysis, those located within 4 Å of the active site, and those involved in the dimer interface were held fixed (fig. S1). The remaining 65 residues of the 153-residue monomer were included in the redesign, allowing them to be changed to any amino acid except cysteine. Thirty-three of the 65 residues subjected to redesign (49%) remained wild-type, a result similar to those of prior applications (*18*, *26*). Sixteen of the point mutations suggested by the program were located on the surface of the protein and were not pursued, whereas the remainder were in the core. The core mutations could be further subdivided into two localized clusters of interacting residues, as well as four additional isolated point mutations (table S1) (*22*).

Site-directed mutagenesis was used to generate each of the two complete clusters of point mutations and the four individual mutations described above. Cluster 1, consisting of nine simultaneous mutations packed between an α helix and several β-strands (including replacement of a buried salt-bridge), aggregated at concentrations above 0.4 mg/mL and was not characterized further. Cluster 2, consisting of four mutations packed between two α helices, remained soluble when concentrated to 20 mg/mL. Individual mutations from this cluster revealed that A23L and I140L (*35*) were key to the thermostabilization of the enzyme and were included in the final construct described below. Of the remaining four individual mutations, one (V108I) was also incorporated in the thermostabilized triple-mutant enzyme, whereas the remaining three (W10T, T67E, and E69L) were not as well behaved and were not characterized further. Both the double mutant (A23L/I140L) and the final triple mutant (A23L/I140L/V108I) were well behaved during expression and purification, more thermostable than the wild-type enzyme, and fully active (table S1) (*22*).

We performed thermal denaturation experiments on all constructs using circular dichroism (CD) spectroscopy (Fig. 1A). Wild-type yCD and the redesigned mutants displayed largely reversible unfolding behavior over the range of temperatures examined; however, at higher temperatures, they unfolded irreversibly (*36*). We quantified the thermal stability of yCD and the mutant constructs by deriving an apparent melting temperature (T_m) from the CD-unfolding curves. This value for the wild-type enzyme was determined to be 52°C. The isolated single mutations A23L, I140L, and V108I each slightly thermostabilized the enzyme, increasing the apparent T_m by ~2°C. However, simultaneous incorporation of all three mutations increased apparent T_m to 62°C, 10°C higher than that of the wild type. Therefore, combination of individual point mutations in a single construct produced a synergistic effect beyond their individual contributions. This result is not simply due to the formation of contacts between redesigned residues, because residue 108 was physically separated from residues 23 and 140.

The kinetic behavior of the wild-type enzyme and the double and triple mutants was measured at 22°C to determine the effects of the mutations (Table 1 and fig. S2), as were their relative activities as a function of temperature (fig. S3). At 22°C, the wild-type enzyme displays a turnover (k_{cat}) of 160 mol (mol enzyme)$^{-1}$ s^{-1} and a Michaelis constant K_m of 1.98 mM, and the double and triple mutants displayed a slightly reduced maximum rate V_{max} coupled with a reduction in the K_m. The catalytic efficiency of the enzyme mutants (expressed as the ratio k_{cat}/K_m) was unchanged relative to the wild-type enzyme. The overall temperature activity profile was broadened, for the redesigned enzyme, with near–wild-type activity retained at lower temperatures and higher activity above 50°C.

The preservation of overall catalytic efficiency (achieved by reducing both k_{cat} and K_m, rather than by maximizing overall velocity) and the unusual change in shape and breadth of the enzyme's thermal profile might suggest that the computational redesign generated mutations that natural or directed evolution pathways might not select, except perhaps as intermediate species. Therefore, computational strategies for thermostabilization might offer a bonus of

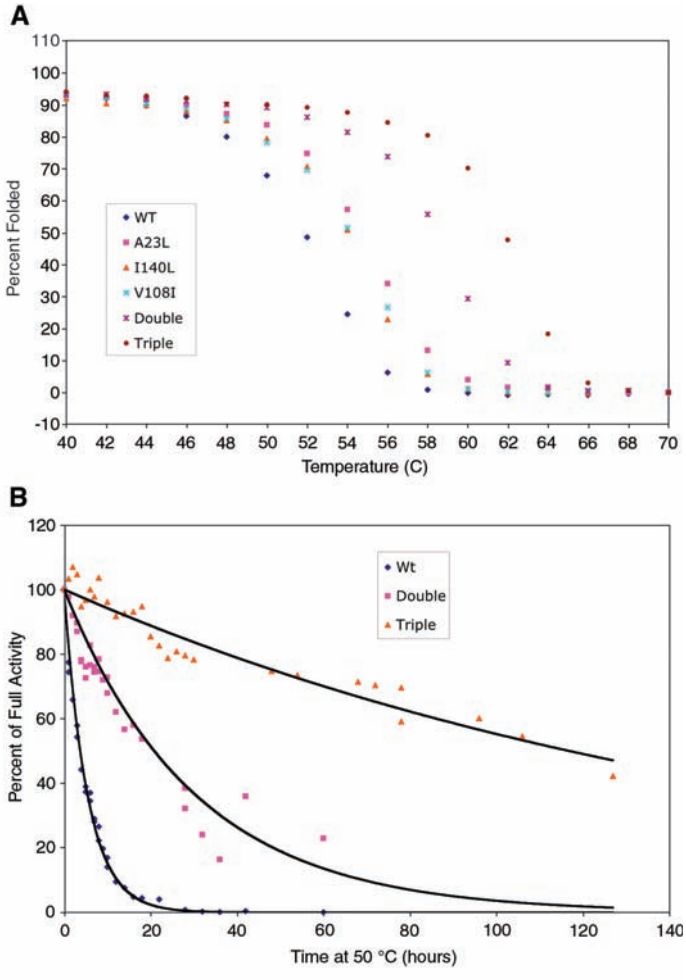

Fig. 1. Thermal denaturation and activity half-life measurements. (**A**) Temperature melt measuring the change in signal at 220 nm over a range of temperatures. All constructs show a folded baseline followed by a sigmodial two-state transition to an unfolded baseline. Only data from 40° to 70° are shown; at lower temperatures, the baseline plateaus corresponded to an assignment of 100% folded protein. (**B**) Activity decay at 50°C. Wild-type yCD and the double and triple mutant constructs were incubated at 50°C, and their activity was measured over time (*32*). The resulting curves gave half-lives for the enzymes at 50°C of 4 hours for the wild type (WT), 21 hours for the double mutant, and 117 hours for the triple mutant.

Table 1. Kinetic behavior of wild-type and redesigned yCD catalysts. Both the double and triple mutants displayed a slightly reduced V_{max}, coupled with a reduction in the Michaelis constant K_m. The catalytic efficiency of the various enzyme mutants (expressed as the ratio k_{cat}/K_m) was unchanged relative to the wild-type enzyme. M prod, molar concentration of product; enz, enzyme.

	Wild type	Double mutant	Triple mutant
K_m (mM)	1.98	1.50	1.33
V_{max} (M prod s^{-1})	0.00016	0.00012	0.00011
k_{cat} (M prod M enz^{-1} s^{-1})	160	120	110
k_{cat}/K_m (M enz^{-1} s^{-1})	80800	80000	82700

selecting mutations that differ in these properties, as compared to selection or redesign experiments based on natural selection.

In order to visualize the time-dependent decay of activity at elevated temperatures, wild-type yCD and the double and triple mutants were incubated at 50°C, and the decrease in their relative activity was monitored over time (Fig. 1B). The wild-type enzyme showed a rapid loss of activity at 50°C, with a half-life of ~4 hours. The double mutant displayed a half-life of ~21 hours, whereas the triple mutant had a half-life at 50°C of ~117 hours (a 30-fold increase over that of the wild type).

In order to determine the effects of the mutations in vivo, a strain of *Escherichia coli* dependent on cytosine deaminase function for uracil synthesis was engineered and transformed with both wild-type and mutant yCD reading frames. Doubling times were then measured at 30°C and 37°C on minimal media lacking uracil (Fig. 2). The thermostabilized mutant construct induced slightly accelerated growth relative to the wild-type enzyme at 30°C and a clear acceleration at 37°C. This suggests that the properties of the engineered variants (a reduced K_M and thermostabilization) measured in vitro correlate with improved enzyme flux in vivo under growth conditions limited by the activity of the enzyme.

The crystal structures of both the double and triple mutants were solved to 1.9 Å and 1.7 Å, respectively. The interpretation of density around the redesigned regions of the protein core (in unbiased omit maps) was unambiguous (fig. S4). The root mean square deviation values comparing the wild-type enzyme and both constructs were under 0.5 Å on all common α carbons and under 0.8 Å on all common atoms. Thus, the redesign and subsequent incorporation of point mutations in the enzyme core had a negligible effect on overall structure of the enzyme, including the active site (fig. S4). The redesigned, mutated residues all appear to pack more tightly in the enzyme core, with more surface area in contact with neighboring residues without altering the nearby side chain rotamers or backbone conformation. Approximately 70 Å^2 of additional buried surface area is incorporated as a result of the three mutations [based on an analysis of residue-by-residue packing, using the program NACCESS (*37*)]. The A23L/I140L double mutation increased the amount of hydrophobic packing against a neighboring tyrosine ring (Fig. 3A), and the addition of V108I in the triple mutant added an additional methyl group to fill a cavity (Fig. 3B).

The stabilized triple mutant was pieced together from part of a cluster of mutations predicted by the program and another single mutation predicted in a separate part of the core. Although the degree of thermostabilization produced by these mutations was relatively modest (an increase for T_m of 2°C for the first change and 4°C for each subsequent mutation), there is no obvious reason why additional mutations predicted by the program could not be iteratively incorporated into the enzyme core, resulting in a panel of catalysts that display sequential increases in thermal stability.

Not all mutations predicted by the program were equally thermostabilizing. Redesigns involving incorporation or alteration of polar or charged residues in the core (such as replacement of a buried salt-bridge in cluster 1 and individual mutations T67E, E69L, and W10T) were less successful than mutations involving substitution of one hydrophobic side chain for another. These latter mutations were predicted and observed to fill cavities within the core with additional van der Waals packing interactions. In future design efforts, selecting mutations of this type in silico may be most successful. Furthermore, modeling of interactions involving buried polar and charged side chains in the enzyme core is an area for future development in computational redesign algorithms.

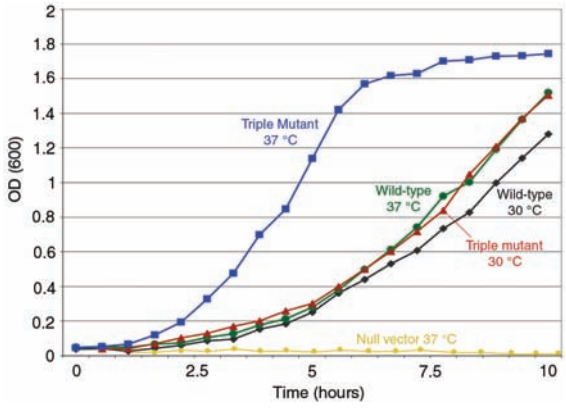

Fig. 2. In vivo assay for metabolic growth phenotype showing bacterial growth curves in media conditions requiring cytosine deaminase activity for generation of uracil (*32*). Both wild-type and reengineered mutants of yCD complement the bacterial activity; the thermostabilized enzyme variant displayed a slight increase in growth rate at 30°C and a clear increase at 37°C. OD (600), optical density at 600 nm.

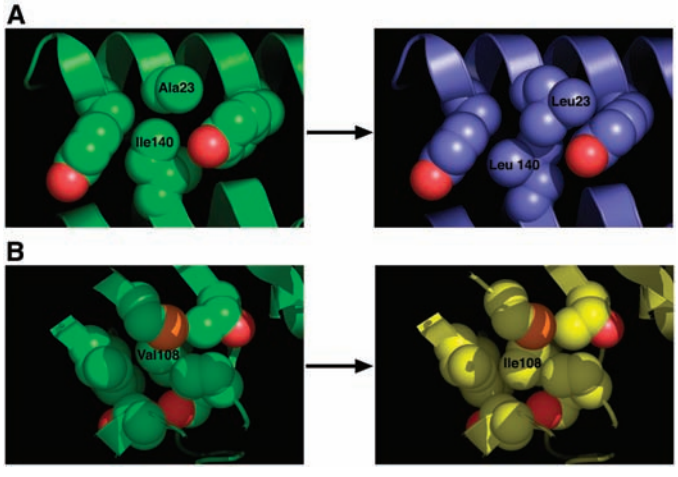

Fig. 3. Structural analyses. (**A**) Van der Waals representation of residues Y19, A23, Y26, and I140 in the wild-type yCD crystal structure (left) and the same representation and orientation for the mutant construct with A23L and I140L mutations (right). (**B**) Van der Waals radii representation of the area around V108 in the wild-type structure (left) and a similar representation of the area around the V108I mutation in the triple mutant crystal structure.

References and Notes

1. V. L. Schramm, *Annu. Rev. Biochem.* **67**, 693 (1998).
2. D. A. Kraut, K. S. Carroll, D. Herschlag, *Annu. Rev. Biochem.* **72**, 517 (2003).
3. R. M. Daniel, R. V. Dunn, J. L. Finney, J. C. Smith, *Annu. Rev. Biophys. Biomol. Struct.* **32**, 69 (2003).
4. V. G. Eijsink *et al.*, *J. Biotechnol.* **113**, 105 (2004).
5. R. Scandurra, V. Consalvi, R. Chiaraluce, L. Politi, P. C. Engel, *Biochimie* **80**, 933 (1998).
6. M. K. Eidsness, K. A. Richie, A. E. Burden, D. M. Kurtz Jr., R. A. Scott, *Biochemistry* **36**, 10406 (1997).
7. D. C. Rees, M. W. Adams, *Structure* **3**, 251 (1995).
8. R. Sterner, W. Liebl, *Crit. Rev. Biochem. Mol. Biol.* **36**, 39 (2001).
9. B. I. Dahiyat, S. L. Mayo, *Science* **278**, 82 (1997).
10. A. G. Street, S. L. Mayo, *Struct. Fold. Des.* **7**, R105 (1999).
11. C. M. Kraemer-Pecore, A. M. Wollacott, J. R. Desjarlais, *Curr. Opin. Chem. Biol.* **5**, 690 (2001).
12. D. B. Gordon, S. A. Marshall, S. L. Mayo, *Curr. Opin. Struct. Biol.* **9**, 509 (1999).
13. J. Mendes, R. Guerois, L. Serrano, *Curr. Opin. Struct. Biol.* **12**, 441 (2002).
14. C. Venclovas, A. Zemla, K. Fidelis, J. Moult, *Proteins* **53** (suppl. 6), 585 (2003).
15. B. I. Dahiyat, *Curr. Opin. Biotechnol.* **10**, 387 (1999).
16. P. Luo *et al.*, *Protein Sci.* **11**, 1218 (2002).
17. S. M. Malakauskas, S. L. Mayo, *Nat. Struct. Biol.* **5**, 470 (1998).
18. G. Dantas, B. Kuhlman, D. Callender, M. Wong, D. Baker, *J. Mol. Biol.* **332**, 449 (2003).
19. D. E. Benson, A. E. Haddy, H. W. Hellinga, *Biochemistry* **41**, 3262 (2002).
20. J. Reina *et al.*, *Nat. Struct. Biol.* **9**, 621 (2002).
21. J. M. Shifman, S. L. Mayo, *J. Mol. Biol.* **323**, 417 (2002).
22. D. T. Berg *et al.*, *Proc. Natl. Acad. Sci. U.S.A.* **100**, 4423 (2003).
23. L. L. Looger, M. A. Dwyer, J. J. Smith, H. W. Hellinga, *Nature* **423**, 185 (2003).
24. B. Kuhlman *et al.*, *Science* **302**, 1364 (2003).
25. M. A. Dwyer, L. L. Looger, H. W. Hellinga, *Science* **304**, 1967 (2004).
26. B. Kuhlman, D. Baker, *Proc. Natl. Acad. Sci. U.S.A.* **97**, 10383 (2000).
27. G. C. Ireton, M. E. Black, B. L. Stoddard, *Structure* **11**, 961 (2003).
28. T. Katsuragi, T. Sonoda, K. Matsumoto, T. Sakai, K. Tonomura, *Agric. Biol. Chem.* **53**, 1313 (1989).

29. E. Kievit *et al.*, *Cancer Res.* **59**, 1417 (1999).
30. M. E. Black, *Genet. Eng. (N.Y.)* **23**, 113 (2001).
31. O. Greco, G. U. Dachs, *J. Cell. Physiol.* **187**, 22 (2001).
32. Materials and methods are available as supporting material on *Science* Online.
33. T. Lazaridis, M. Karplus, *Proteins* **35**, 133 (1999).
34. R. L. Dunbrack Jr., F. E. Cohen, *Protein Sci.* **6**, 1661 (1997).
35. Single-letter abbreviations for the amino acid residues are as follows: A, Ala; C, Cys; D, Asp; E, Glu; F, Phe; G, Gly; H, His; I, Ile; K, Lys; L, Leu; M, Met; N, Asn; P, Pro; Q, Gln; R, Arg; S, Ser; T, Thr; V, Val; W, Trp; and Y, Tyr.
36. A. Korkegian, M. E. Black, D. Baker, B. L. Stoddard, unpublished data.
37. S. J. Hubbard, J. M. Thornton, NACCESS (Department of Biochemistry and Molecular Biology, Univ. College London, 1993), available at http://wolf.bms.umist.ac.uk/naccess.
38. The authors acknowledge the assistance and advice of the Baker Laboratory in running RosettaDesign, the FHCRC structural biology program for assistance with data collection, and critiques and suggestions from R. Strong and A. Ferre-D'Amare. Funding was provided by NIH grant nos. GM49857 and CA97328 (B.L.S.), CA97328 and CA85939 (M.E.B.), GM59224 (D.B.), and T32-GM08268 (A.K.). Crystal structures of the yCD double and triple mutants have been submitted to the Research Collaboratory for Structural Bioinformatics Protein Databank with accession codes 1YSD and 1YSB, respectively.

Supporting Online Material
www.sciencemag.org/cgi/content/full/308/5723/857/DC1
Materials and Methods
Figs. S1 to S4
Table S1
References and Notes

10 November 2004; accepted 16 February 2005
10.1126/science.1107387

Swimming Against the Flow: A Mechanism of Zooplankton Aggregation

Amatzia Genin,[1]* Jules S. Jaffe,[2] Ruth Reef,[1] Claudio Richter,[3] Peter J. S. Franks[2]

Zooplankton reside in a constantly flowing environment. However, information about their response to ambient flow has remained elusive, because of the difficulties of following the individual motions of these minute, nearly transparent animals in the ocean. Using a three-dimensional acoustic imaging system, we tracked >375,000 zooplankters at two coastal sites in the Red Sea. Resolution of their motion from that of the water showed that the animals effectively maintained their depth by swimming against upwelling and downwelling currents moving at rates of up to tens of body lengths per second, causing their accumulation at frontal zones. This mechanism explains how oceanic fronts become major feeding grounds for predators and targets for fishermen.

Buoyant phytoplankton and nonliving flotsam accumulate at the sea surface along convergent fronts because they remain afloat while the water submerges (*1*, *2*). Accumulations at fronts have also been reported for zooplankton (*3*, *4*); however, their aggregations often occur below the surface and at both convergent (downwelling) and divergent (upwelling) zones (*5*). Hardy (*6*) was the first to suggest that such patchiness must be caused by some dynamic principles involving zooplankton behavior and water movement. A common, yet untested explanation for subsurface accumulations at frontal zones is that the animals actively swim against vertical currents in an attempt to maintain their depth (*5*, *7*–*10*). Models (*7*, *8*) show that complete depth retention by zooplankton should generate increasingly dense accumulations, whereas partial retention, due to fatigue or inability to match the velocity of the current, should lead to ephemeral patches. Copepods can form fine-scale aggregations in layers where the turbulence velocity is substantially weaker than their typical swimming speed (*11*). Although diel vertical migrations are well known among zooplankton in response to seasonal cues, their behavioral response to ambient currents has not been demonstrated in the ocean, largely because of the lack of a technology that can track in situ the motions of these small, nearly transparent organisms in a large volume of water.

We tested the hypothesis that zooplankton swim against vertical currents by acoustically tracking animals while simultaneously measuring currents at two coastal sites in the northern Gulf of Aqaba, Red Sea (table S1). The sites experience persistent (hours-long) periods of upwelling and downwelling driven by differential heating and cooling across the gradually sloping bottom (*12*, *13*) and by the interaction between mesoscale currents and coastal topography. The three-dimensional trajectories of individual zooplankters as small as 1 mm in length were measured with FishTV-1.6 (FTV-1.6), a new, high-frequency (1.6-MHz), multibeam sonar (*14*), within volumes of water up to 3.8 m in length and 0.1 to 0.4 m in width (Fig. 1) (*15*). The sonar's transducer, attached to a large submerged tripod (Fig. 1), was varied in depth and orientation among deployments (table S1). Three experiments using FTV-1.6 accomplished 274 tracking sessions, most of them acquiring >10 min of uninterrupted bioacoustic data at a rate of three "frames" per second, yielding a total of 375,171 tracks. The sessions were performed day and night under conditions of upwelling and downwelling currents (table S1).

Vertical and horizontal currents at the depth of the insonified volume were measured nearby (<15 m) during each tracking session (Fig. 1) (*15*). The average vertical flow during the three experiments, approximately 1 cm/s, was 10 to 15% of the prevailing horizontal currents.

Net tows near the insonified volume indicated that during the day, zooplankton assemblages consisted mostly of pelagic species typical of the open waters of the Red Sea (*16*). At night, the emergence of demersal zooplankton doubled the zooplankton density (*17*). At all times, copepods were the dominant group (50 to 85% by number). Additional common taxa included mollusks, chaetognaths, and tunicates; and during the night, decapod larvae and other crustaceans. More than 70% of the targets recorded by FTV-1.6 had weak reflectivity (<–80 dB referenced to 1 μPa at 1 m range), in agreement with the dominance in the net samples of small (<5 mm) zooplankton from the aforementioned taxa.

Comparison of the tracks obtained from the sonar with the currents revealed that under both downwelling and upwelling conditions, the zooplankton swam against the vertical currents (Fig. 2 and Table 1). Complete depth retention, with a regression coefficient of –1.0 between the zooplankton's vertical swimming velocity (V_z, relative to water) and the vertical current (V_w), was found in the first and second experiments; and nearly complete retention ($V_z = -0.82\ V_w$) was found in the third experiment (Table 1). These results indicated that under strong vertical velocities, the small zooplankton recorded with FTV-1.6 swam vertically at velocities of >10 body lengths/s. In contrast, the animals' mean horizontal displacement (H_z) was indistinguishable from that of the current (H_w), with a regression coefficient of 1.0 ($H_z = H_w$) in the first and second experiments, indicating that the animals were passively drifting with horizontal currents; and nearly so ($H_z = 0.73\ H_w$) in the third experiment (Fig. 2).

Planktonic organisms that maintain their depth are expected to accumulate where vertical currents persist (*7*, *8*). Because shallow downwelling and upwelling zones at the study sites were confined to near-shore waters (*12*, *13*), a greater abundance of zooplankton was expected near the coast (movie S1). To test this prediction, we examined the distri-

[1]The Interuniversity Institute for Marine Sciences and the Hebrew University, Eilat, Israel. [2]Scripps Institution of Oceanography, La Jolla, CA, USA. [3]Center for Tropical Marine Ecology, Bremen, Germany.

*To whom correspondence should be addressed. E-mail: amatzia@vms.huji.ac.il